CALCIUM AND PROTON DEPENDENCE OF SARCOPLASMIC RETICULUM ATPASE

GIUSEPPE INESI
Department of Biological Chemistry, University of Maryland Medical School, Baltimore, Maryland 21201

TERRELL L. HILL
Laboratory of Molecular Biology, National Institutes of Arthritis, Diabetes, and Digestive and Kidney Diseases, National Institutes of Health, Bethesda, Maryland 20205

ABSTRACT The influence of Ca^{2+} and H^+ concentrations on the sequential reactions of the ATPase cycle was studied by a series of pre-steady state and steady state experiments with sarcoplasmic reticulum vesicles. It is shown that H^+ competition with calcium binding results in a reduced population of activated enzyme, which is manifested by a lower level of phosphorylated enzyme intermediate following addition of ATP. Further effects of Ca^{2+} and H^+ are demonstrated on the progression of the phosphoenzyme through the reaction cycle and on the final hydrolytic cleavage of Pi. The overall dependence of steady state ATP flux on Ca^{2+} and H^+ concentrations in leaky vesicles is expressed by a series of curves showing that as the H^+ concentration is raised higher Ca^{2+} concentrations are required to obtain half-maximal ATP fluxes. At saturating Ca^{2+}, maximal ATP fluxes are observed at an intermediate H^+ concentration (pH 7.2), while lower levels are obtained as the H^+ concentration is reduced (to pH 8) or increased (to pH 6). A preliminary model is then proposed based on the presence of two interacting domains permitting competitive binding of Ca^{2+} or H^+, per each catalytic site undergoing phosphorylation by ATP. The model considers three main states and thirteen substates (depending on the occupancy of the binding sites in each state by Ca^{2+}, H^+, or neither) in the progression of the ATP cycle, coupled to transport of Ca^{2+} and counter transport of H^+ in leaky vesicles. Considering the preliminary nature of the model and the experimental scatter, a rather satisfactory agreement is noted between a family of curves generated by theoretical analysis and the ATP flux curves obtained experimentally.

INTRODUCTION

The catalytic and transport cycle of sarcoplasmic reticulum (SR)ATPase, including initial calcium binding, ATP utilization for formation of a phosphorylated enzyme intermediate, inward calcium translocation, and hydrolytic cleavage of the phosphoenzyme can be illustrated with the aid of a reaction scheme adapted from deMeis and Vianna (1). In our adaptation of the scheme (Fig. 1), E denotes enzyme states with high-affinity calcium sites exposed on the outer surface ofthe SR vesicles, one asterisk (*) denotes a state with low-affinity calcium sites exposed to the inner surface of the vesicles, and two asterisks (**) denotes states with low-affinity calcium sites exposed to the outer surface of the vesicles. In addition, we introduce Ca^{2+} vs. H^+ exchange. T, α, and β correspond to enzyme states to be defined later.

Calcium binding to specific sites of E is an absolute requirement for enzyme activation, which is coupled to active transport of the divalent cation. At equilibrium and in the absence of ATP, calcium binding occurs with a cooperative behavior and is accompanied by a protein conformational change (2). Furthermore, the affinity of the ATPase for Ca^{2+} and the cooperative character of binding are profoundly influenced by the H^+ concentration in the medium. Such a dependence has been explained with a mechanism involving competition of one Ca^{2+} and one H^+ for each binding site, and cooperative interaction of the binding domains (3). An important question then, is whether or not these events play a role in the catalytic and transport activity sustained by the enzyme upon addition of ATP. Although, in general, pH dependences of enzyme activities may be attributed to nonspecific protein titration, we present here a set of experimental findings demonstrating specific H^+ effects on various steps of the ATPase reaction. Based on these findings, we then provide a preliminary model for analysis of the dependence of steady state enzyme activity on Ca^{2+} and H^+ concentrations.

EXPERIMENTAL METHODS

SR vesicles were obtained from rabbit hind leg muscle as previously described (4). In rapid kinetic experiments, enzyme phosphorylation and Pi production were initiated by mixing SR vesicles with (γ-^{32}P) ATP in the appropriate medium, and the reaction was then quenched at serial times in 3.5% Cl_3CCOOH and 0.1 mM Pi. Both initial mixing and quenching were carried out in a Durrum multimixing apparatus (Dionex Corp., Sunnyvale, CA). ^{32}P-phosphoenzyme and ^{32}P-Pi were measured as

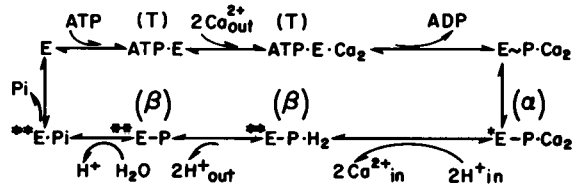

FIGURE 1 Diagram illustrating the catalytic and transport cycle of SR ATPase.

in reference 2. Calcium transport was measured under identical conditions. In this case, however, a radioactive calcium tracer (^{45}Ca) was used, and the reaction was quenched with EGTA (10 mM EGTA, 10 mM $MgCl_2$, 80 mM KCl, and 20 mM MOPS pH 6.8 with or without 6 mM ADP) instead of the acid quencher; 0.5 ml of the quenched mixture was passed through a HATF 0.45 μm Millipore filter (Millipore/Continental Water Systems, Bedford, MA), which was washed with cooled quenching solution and dissolved for determination of radioactivity.

The kinetics of hydrolytic cleavage of the phosphoenzyme were studied by first equilibrating SR vesicles with ^{32}P-Pi inthe absence of Ca^{2+} for 5–10 min to obtain formation of ^{32}P-phosphoenzyme. This reaction mixture was then diluted with excess nonradioactive Pi and ATP, and then quenched at serial times with perchloric acid and nonradioactive Pi (final concentrations 125 and 2 mM). The residual ^{32}P-phosphoenzyme was measured as in reference 2. Steady state ATPase activity was followed by determination of Pi production by the molybdovanadate reaction (5).

Proton fluxes were measured under identical conditions with the aid of a Dionex Corp. D-137 dual-detector stopped-flow spectrophotometer; 630- and 577-nm filters were chosen. The spectrophotometer was interfaced with a Northstar Horizoncomputer, which was programmed to store, amplify, and subtract series of data for oscilloscope display. Syringe A contained the SR solution supplemented or not with 0.2% Triton X-100 (leaky and intact vesicles, respectively), and syringe B contained buffer solution supplemented or not with ATP (500 μM).

The protein concentration was measured by the Folin method standardized with bovine serum albumin. Total calcium was measured by double wavelength photometry and titration with EGTA in the presence of the metallochromic indicator, murexide. Estimates of free Ca^{2+} were computed taking into account pH and concentrations of ATP, K^+, and Mg^{2+}. The absolute $EGTA^{4-}\cdot Ca^{2+}$ binding constant (log K = 10.716) given by Allen et al. (6) was used in these calculations, as discussed by Fabiato and Fabiato (7).

EXPERIMENTAL OBSERVATIONS

Transient State Experiments

The experiments illustrated in Figs. 2 and 3 deal with pre-steady state phenomena of the ATPase cycle. Addition of ATP to SR vesicles in the presence of Ca^{2+} results in the transfer of the ATP terminal phosphate onto an aspartyl residue at the catalytic site and formation of phosphorylated enzyme intermediate (8–11). The stoichiometric relation of the initial calcium binding to the phosphorylation sites is 2:1 (2), and the time course of enzyme phosphorylation following addition of ATP can be resolved by rapid quench methods (12, 13). We show there that in analogy to the competitive effect of H^+ on calcium binding as measured directly in equilibrium conditions (3), enzyme phosphorylation by ATP in the presence of 0.8–8.0 μM Ca^{2+} is competitively inhibited by H^+ (Fig. 2). It is thereby demonstrated that the previously described competiton

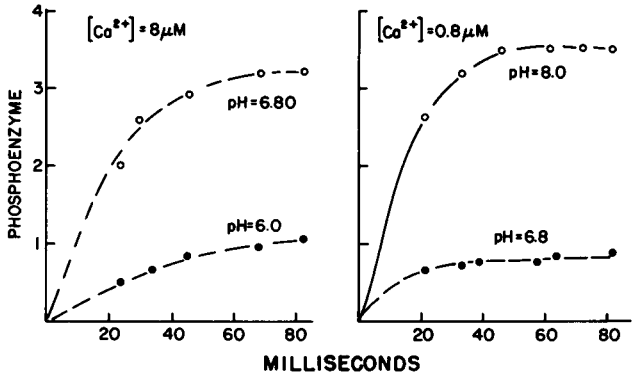

FIGURE 2 Enzyme phosphorylation following addition of ATP, in the presence of various Ca^{2+} and H^+ concentrations. Equal volumes of 20 mM Tris-maleate (pH as indicated), 80 mM KCl, 5 mM $MgCl_2$, 0.5 mM $CaCl_2$, EGTA to yield free Ca^{2+} as indicated, and either 0.3 mg SR protein/ml or 10 μM (γ-^{32}P) ATP were mixed toinitiate the reaction. Acid quenching at serial times was then carried out as described in the section on methods. Temperature, 25°C.

between H^+ and Ca^{2+} does in fact involve binding sites whose occupancy by calcium is a strict requirement for enzyme phosphorylation by ATP.

The observed rate constant for formation of the phosphorylated enzyme intermediate is at least one order of magnitude higher than the enzyme turnover (12, 13). Therefore the phosphoenzyme can reach levels nearly equal to the total number of catalytic sites (4 nm/mg protein). We find that in the presence of relatively high Ca^{2+} concentrations (100 μM), maximal levels of phosphoenzyme are obtained within 20 ms following addition of saturating ATP, independent of variations of H^+ concentrations from 10^{-8} to 10^{-6} M (Fig. 3). This indicates that phosphorylation of the enzyme with ATP is not interferred with by H^+, if the Ca^{2+} concentration in the medium is raised to levels that are sufficient to overcome H^+ competition for binding sites on the enzyme-ATP complex (T state in Fig. 1).

Enzyme phosphorylation with ATP is rapidly followed by translocation of two moles of calcium per mole of phosphorylated enzyme intermediate (14). This phenomenon is kinetically distinct and appears as a rapid burst preceding steady state transport activity. The calcium involved in the initial burst (i.e., extrapolation of the steady state calcium uptake to the vertical axis of Fig. 3) is not immediately released into the lumen of the vesicles, but is maintained in an occluded state (15) for a finite time of the ATPase cycle (α state in Fig. 1).

We find now that the initial burst of calcium translocation, as detected by EGTA quenching, includes two roughly equivalent components: One component is released when ADP is added with EGTA to the quenching medium and another component remains associated with the vesicles even following ADP·EGTA quenching (Fig. 3). Because the initial calcium burst is related with a stoichiometric ratio of 2:1 to the phosphoenzyme level, it is

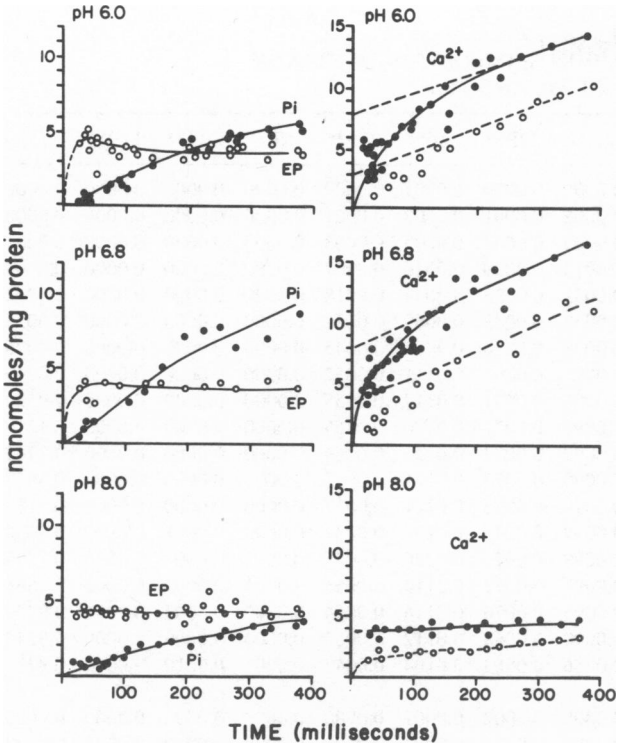

FIGURE 3 Enzyme phosphorylation, calcium translocation, and Pi production following addition of ATP, in the presence of saturating Ca^{2+} and various H^+ concentrations. Equal volumes of 20 mM Tris-maleate (pH as indicated), 80 mM KCl, 5 mM $MgCl_2$, 100 μM $CaCl_2$ (^{45}Ca tracer for the calcium translocation experiments), and either 0.6 mg SR protein/ml, or 200 μM ATP ([γ-^{32}P] ATP for the phosphorylation and Pi production experiments) were mixed to initiate the reaction. Acid (for the phosphorylation experiments), acid EGTA (•), or EGTA and ADP (○) quenching (for the Ca^{2+} translocation experiments) was obtained at serial times as described in section on methods. Temperature, 25°C.

apparent that in the transient state the phosphoenzyme shifts between one state that is reactive to ADP and one that is not. (We take into consideration the distribution of intermediates during the steady state, see Table I.)

At acid and neutral pH, the initial burst is followed by steady state calcium transport concomitant to Pi release. At alkaline pH, we find that the initial calcium translocation is limited to the ADP-sensitive component, and very little transport is detected following the initial burst (Fig. 3). Furthermore, Pi production is very low in spite of the presence of high phosphoenzyme levels. These transient-state experiments indicate a H^+ requirement for evolution of the enzyme cycle following phosphorylation and the initial burst of calcium internalization.

The last partial reaction of the catalytic cycle is hydrolytic cleavage of the phosphoenzyme. The effect of H^+ on the hydrolytic reaction that releases Pi from the phosphorylated ATPase can be studied directly by using enzyme phosphorylated with ^{32}Pi (16) in the absence of Ca^{2+} (formation of β state in the reverse direction of the cycle in Fig. 1). In this manner the hydrolytic reaction is isolated from intermediate steps related to evolution of the phosphoenzyme formed with ATP in the presence of Ca^{2+}. Following enzyme phosphorylation with ^{32}Pi the reaction mixture is diluted with excess nonradioactive Pi, ATP, and a buffer yielding the appropriate pH. The reaction is then quenched with acid at serial times to measure residual ^{32}P-phosphoenzyme. It is shown in Fig. 4 that, within the pH range 6 to 8, the hydrolytic reaction proceeds with an apparent rate constant that is 5–6 times higher than the enzyme turnover (Fig. 5). Furthermore, the hydrolytic reaction occurs at a lower rate in the presence of high H^+ concentrations (pH 6.0), indicating that the protonated species of state β has a lower rate constant than the dissociated species.

Considering the relatively high rate constants of the hydrolytic reaction, and the absence of a pre-steady state burst of Pi production (Fig. 3), it is apparent that progression of state α to state β (Fig. 1) contributes significantly to rate limitation for the enzyme turnover. Because we find that, in the presence of identical levels of phosphorylated enzyme intermediate, the steady state ATPase activity is inhibited by a reduction of the H^+ concentration (pH 8 in Fig. 3), we conclude tht progression state α to state β is favored by a high H^+ concentration.

Steady State Experiments

The complex dependence of the steady-state ATPase activity on Ca^{2+} and H^+ concentrations is shown in Fig. 5. For these measurements, the SR vesicles were exposed to a divalent cation ionophore to induce calcium leak and avoid "back inhibition" by high intravesicular Ca^{2+}. Furthermore, SR vesicles are highly permeable to H^+ (17). Therefore, constant rates of Pi production were obtained in the presence of saturating ATP concentrations. Inspection of Fig. 5 reveals that when the H^+ concentration is raised, higher Ca^{2+} concentrations are required to obtain half-maximal ATPase fluxes. This is due to H^+ competition with Ca^{2+} for the activating sites, resulting in a lower population of activated enzyme, as shown in Fig. 2. Furthermore, in the presence of Ca^{2+} concentrations producing maximal occupancy of binding sites on the enzyme-ATP complex (T state), highest ATPase fluxes are observed at intermediate H^+ concentrations (pH 7.2).

A nearly identical maximal flux of ATP, and a similar pattern of H^+ and Ca^{2+} dependence, were obtained when these experiments were repeated at lower (2 mM as opposed to 9 mM) Mg^{2+} concentration. Although the apparent affinity of the ATP for Ca^{2+} is somewhat higher at low Mg^{2+} concentrations, we consider here the set of date obtained at high Mg^{2+} to be consistent with our previous measurements of calcium binding at equilibrium in the absence of ATP (3).

In the light of the findings described above, we suggest that inhibition of the maximal ATP flux at low (pH 8) and high (pH 6) H^+ concentrations, is related to a low population of protonated α state (limiting the hydrolytic reaction) in the latter case.

TABLE I
CALCULATED DISTRIBUTION OF ENZYME INTERMEDIATES IN STEADY STATE AS A FUNCTION OF pH AND pCa

pH	pCa	J	T	11P*	10P*	00P*	12P*	02P*	22P*	22P**	02P**	00P**	12P**	10P**	11P**	f_{11T}
8.0	7.75	0.0127	0.9952	0.0000	0.0001	0.0045	0.0000	0.0000	0.0000	0.0000	0.0001	0.0000	0.0000	0.0000	0.0000	0.0000
	7.50	0.0393	0.9850	0.0001	0.0002	0.0138	0.0001	0.0001	0.0002	0.0001	0.0002	0.0001	0.0000	0.0000	0.0000	0.0000
	7.25	0.1186	0.9547	0.0004	0.0007	0.0418	0.0004	0.0004	0.0005	0.0003	0.0006	0.0003	0.0000	0.0000	0.0000	0.0001
	7.00	0.3338	0.8726	0.0010	0.0019	0.1176	0.0012	0.0012	0.0013	0.0009	0.0016	0.0007	0.0000	0.0000	0.0000	0.0004
	6.75	0.8019	0.6939	0.0025	0.0047	0.2826	0.0028	0.0028	0.0031	0.0023	0.0038	0.0018	0.0000	0.0000	0.0000	0.0012
	6.50	1.4759	0.4366	0.0045	0.0086	0.5201	0.0052	0.0051	0.0057	0.0042	0.0069	0.0032	0.0000	0.0000	0.0000	0.0035
	6.25	2.0489	0.2178	0.0063	0.0120	0.7219	0.0072	0.0071	0.0078	0.0058	0.0096	0.0045	0.0000	0.0000	0.0000	0.0096
	6.00	2.3646	0.0972	0.0072	0.0139	0.8331	0.0084	0.0082	0.0091	0.0067	0.0111	0.0052	0.0000	0.0000	0.0000	0.0249
	5.75	2.5037	0.0438	0.0077	0.0149	0.8819	0.0091	0.0087	0.0096	0.0071	0.0117	0.0055	0.0000	0.0000	0.0000	0.0584
	5.50	2.5613	0.0215	0.0079	0.0156	0.9019	0.0096	0.0089	0.0098	0.0072	0.0120	0.0056	0.0000	0.0000	0.0000	0.1219
	5.25	2.5848	0.0118	0.0079	0.0164	0.9098	0.0102	0.0090	0.0099	0.0073	0.0121	0.0056	0.0000	0.0000	0.0000	0.2243
	5.00	2.5933	0.0073	0.0080	0.0177	0.9119	0.0111	0.0090	0.0099	0.0073	0.0121	0.0057	0.0000	0.0000	0.0000	0.3627
	4.75	2.5933	0.0051	0.0080	0.0197	0.9104	0.0127	0.0090	0.0099	0.0073	0.0121	0.0057	0.0000	0.0000	0.0000	0.5184
	4.50	2.5861	0.0040	0.0080	0.0233	0.9052	0.0155	0.0090	0.0099	0.0073	0.0121	0.0057	0.0000	0.0001	0.0000	0.6650
	4.25	2.5697	0.0034	0.0080	0.0296	0.8949	0.0203	0.0089	0.0098	0.0073	0.0120	0.0056	0.0001	0.0001	0.0000	0.7829
	4.00	2.5391	0.0030	0.0081	0.0403	0.8764	0.0287	0.0088	0.0097	0.0072	0.0119	0.0056	0.0001	0.0002	0.0000	0.8665
	3.75	2.4849	0.0028	0.0084	0.0583	0.8449	0.0428	0.0086	0.0095	0.0070	0.0116	0.0054	0.0002	0.0004	0.0000	0.9208
	3.50	2.3923	0.0026	0.0094	0.0873	0.7933	0.0657	0.0083	0.0092	0.0068	0.0112	0.0052	0.0004	0.0006	0.0000	0.9540
	3.25	2.2398	0.0023	0.0124	0.1307	0.7142	0.1006	0.0078	0.0086	0.0063	0.0104	0.0049	0.0007	0.0010	0.0000	0.9737
7.2	7.75	0.0107	0.9991	0.0000	0.0000	0.0003	0.0002	0.0000	0.0000	0.0002	0.0001	0.0000	0.0000	0.0000	0.0000	0.0000
	7.50	0.0330	0.9974	0.0001	0.0001	0.0008	0.0003	0.0000	0.0001	0.0006	0.0003	0.0000	0.0000	0.0000	0.0000	0.0000
	7.25	0.1000	0.9920	0.0003	0.0004	0.0024	0.0017	0.0001	0.0004	0.0017	0.0009	0.0001	0.0000	0.0000	0.0000	0.0001
	7.00	0.2927	0.9766	0.0009	0.0013	0.0071	0.0049	0.0002	0.0011	0.0050	0.0026	0.0003	0.0000	0.0000	0.0000	0.0003
	6.75	0.8016	0.9358	0.0025	0.0036	0.0195	0.0135	0.0004	0.0031	0.0137	0.0070	0.0009	0.0000	0.0000	0.0000	0.0009
	6.50	1.9502	0.8439	0.0060	0.0087	0.0474	0.0329	0.0011	0.0075	0.0334	0.0171	0.0021	0.0000	0.0000	0.0000	0.0024
	6.25	3.9540	0.6835	0.0121	0.0176	0.0961	0.0668	0.0022	0.0151	0.0676	0.0348	0.0042	0.0000	0.0000	0.0000	0.0059
	6.00	6.4397	0.4844	0.0197	0.0286	0.1565	0.1088	0.0035	0.0247	0.1102	0.0566	0.0069	0.0000	0.0000	0.0000	0.0136
	5.75	8.6401	0.3081	0.0265	0.0385	0.2099	0.1462	0.0048	0.0331	0.1478	0.0759	0.0093	0.0000	0.0000	0.0000	0.0287
	5.50	10.1653	0.1856	0.0312	0.0453	0.2469	0.1723	0.0056	0.0389	0.1739	0.0893	0.0109	0.0000	0.0000	0.0000	0.0560
	5.25	11.0885	0.1109	0.0340	0.0496	0.2691	0.1887	0.0061	0.0425	0.1897	0.0975	0.0119	0.0001	0.0000	0.0000	0.1021
	5.00	11.6093	0.0679	0.0356	0.0522	0.2814	0.1988	0.0064	0.0445	0.1986	0.1020	0.0124	0.0001	0.0000	0.0000	0.1747
	4.75	11.8838	0.0435	0.0365	0.0540	0.2874	0.2057	0.0065	0.0455	0.2033	0.1044	0.0127	0.0003	0.0001	0.0000	0.2788
	4.50	12.0032	0.0298	0.0369	0.0554	0.2892	0.2118	0.0066	0.0460	0.2053	0.1055	0.0129	0.0005	0.0001	0.0000	0.4110
	4.25	12.0094	0.0221	0.0370	0.0571	0.2873	0.2189	0.0066	0.0460	0.2054	0.1055	0.0129	0.0009	0.0002	0.0000	0.5559
	4.00	11.9088	0.0176	0.0369	0.0595	0.2814	0.2293	0.0066	0.0456	0.2037	0.1047	0.0128	0.0015	0.0004	0.0000	0.6910
	3.75	11.6788	0.0149	0.0366	0.0631	0.2702	0.2457	0.0064	0.0447	0.1997	0.1026	0.0125	0.0027	0.0007	0.0000	0.7995
	3.50	11.2733	0.0131	0.0362	0.0688	0.2515	0.2712	0.0062	0.0432	0.1928	0.0991	0.0121	0.0046	0.0013	0.0000	0.8766
	3.25	10.6344	0.0117	0.0358	0.0769	0.2235	0.3089	0.0059	0.0407	0.1819	0.0934	0.0114	0.0077	0.0021	0.0001	0.9267
6.0	7.75	0.0019	0.9997	0.0000	0.0000	0.0000	0.0001	0.0000	0.0000	0.0002	0.0000	0.0000	0.0000	0.0000	0.0000	0.0000
	7.50	0.0056	0.9992	0.0000	0.0000	0.0000	0.0003	0.0000	0.0000	0.0005	0.0000	0.0000	0.0000	0.0000	0.0000	0.0000
	7.25	0.0165	0.9975	0.0001	0.0000	0.0000	0.0009	0.0000	0.0001	0.0014	0.0001	0.0000	0.0000	0.0000	0.0000	0.0000
	7.00	0.0459	0.9931	0.0001	0.0000	0.0000	0.0024	0.0000	0.0002	0.0040	0.0001	0.0000	0.0000	0.0000	0.0000	0.0000
	6.75	0.1190	0.9821	0.0004	0.0001	0.0000	0.0063	0.0000	0.0005	0.0103	0.0004	0.0000	0.0000	0.0000	0.0000	0.0001
	6.50	0.2814	0.9576	0.0009	0.0002	0.0001	0.0148	0.0000	0.0011	0.0245	0.0009	0.0000	0.0000	0.0000	0.0000	0.0003
	6.25	0.5976	0.9100	0.0018	0.0005	0.0002	0.0314	0.0000	0.0023	0.0519	0.0018	0.0000	0.0000	0.0000	0.0000	0.0007
	6.00	1.1318	0.8295	0.0035	0.0010	0.0003	0.0595	0.0000	0.0043	0.0984	0.0034	0.0000	0.0000	0.0000	0.0000	0.0014
	5.75	1.9082	0.7126	0.0058	0.0017	0.0005	0.1003	0.0001	0.0073	0.1659	0.0058	0.0001	0.0000	0.0000	0.0000	0.0027
	5.50	2.8680	0.5680	0.0088	0.0025	0.0007	0.1508	0.0001	0.0110	0.2493	0.0087	0.0001	0.0000	0.0000	0.0000	0.0052
	5.25	3.8680	0.4174	0.0119	0.0034	0.0010	0.2033	0.0001	0.0148	0.3362	0.0117	0.0001	0.0000	0.0000	0.0000	0.0095
	5.00	4.7502	0.2845	0.0146	0.0041	0.0012	0.2497	0.0002	0.0182	0.4129	0.0144	0.0001	0.0000	0.0000	0.0000	0.0171
	4.75	5.4237	0.1830	0.0166	0.0047	0.0014	0.2852	0.0002	0.0208	0.4715	0.0165	0.0001	0.0000	0.0000	0.0000	0.0303
	4.50	5.8837	0.1135	0.0180	0.0051	0.0015	0.3095	0.0002	0.0225	0.5114	0.0179	0.0002	0.0001	0.0000	0.0000	0.0529
	4.25	6.1741	0.0695	0.0189	0.0054	0.0016	0.3249	0.0002	0.0237	0.5367	0.0188	0.0002	0.0002	0.0000	0.0000	0.0907
	4.00	6.3473	0.0429	0.0195	0.0055	0.0016	0.3344	0.0002	0.0243	0.5517	0.0193	0.0002	0.0003	0.0000	0.0000	0.1510
	3.75	6.4450	0.0274	0.0198	0.0056	0.0017	0.3401	0.0002	0.0247	0.5602	0.0196	0.0002	0.0005	0.0000	0.0000	0.2405
	3.50	6.4946	0.0184	0.0200	0.0057	0.0017	0.3437	0.0002	0.0249	0.5645	0.0197	0.0002	0.0009	0.0000	0.0000	0.3604
	3.25	6.5112	0.0133	0.0202	0.0057	0.0016	0.3463	0.0002	0.0249	0.5660	0.0198	0.0002	0.0017	0.0000	0.0000	0.5006

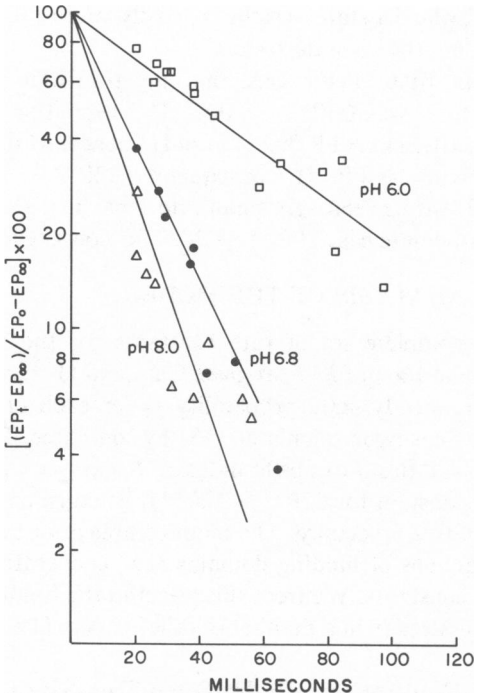

FIGURE 4 Decay of ^{32}P-phosphoenzyme at various H^+ concentrations. ^{32}P-phosphoenzyme was obtained by equilibrating SR vesicles (1.0 mg protein/ml) with 2.0 mM ^{32}P-Pi in 5 mM Tris-maleate (pH 6.0), 15 mM $MgCl_2$ and 0.5 mM EGTA-Tris. Following 5–10 min incubation, the reaction mixture was diluted with an equal volume of 40 mM Tris-maleate (pH as indicated), 160 mM KCl, 2 mM ATP, and 25 mM (nonradioactive) Pi. Acid quenching at serial times was then obtained as described in the reaction on methods. Temperature, 25°C.

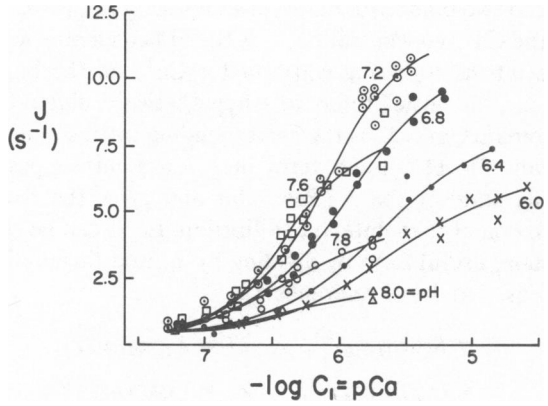

FIGURE 5 Steady state ATP flux in leaky vesicles at variable H^+ and Ca^+ concentrations. The reaction was initiated by addition of 1 mM (final concentration) ATP to a mixture containing 10 mM Tris-maleate (pH as indicated), 10 mM $MgCl_2$, 80 mM KCl, 40–50 μM total calcium, EGTA to yield free Ca^{2+} as indicated, 10 μM A21837 (a divalent cation ionophore used to produce leaky vesicles),and 50–100 μM SR protein/ml. The reaction was then quenched at serial times with the molybdovanadate reagent (5), and Pi was determined by colorimetry. The ATP flux was obtained from the slope of Pi production as a function of time, and related to one enzyme unit (4 nmol enzyme/mg protein in our preparation). Temperature, 25°C.

THE MODEL

Our object here is to suggest a preliminary model to account semiquantitatively for the family of ATP flux curves in Fig. 5. There remain a number of uncertainties about the ingredients that should be included in such a model. Therefore, it would be premature to make elaborate calculations for a full model. In particular, we limit ourselves to calculations based on an ATPase unit comprising two calcium sites and one phosphorylation site, with no reference to whether the unit consists of one or two polypeptide chains. We do not consider larger complexes such as a four-site unit, which we introduced in our previous analysis of equilibrium binding of Ca^{2+} and H^+ to SR ATPase (3). The two-site unit is adequate to illustrate our approach and to provide rather good agreement with the experimental findings. As will be seen below, there are 13 states and 9 interaction parameters in the final kinetic diagram that we use for a dimer. For a four-site unit treated in an analogous way, there would be 216 states and many new (hybrid) interaction parameters.

Of the various species represented in Fig. 1, E is the only enzyme species considered in our previous paper on equilibrium binding of Ca^{2+} and H^+ in the absence of ATP. There was no difficulty in using a four-site model for this equilibrium problem (in fact a two-site unit would not have provided strong enough cooperativity). In our model of steady state ATP flux here, we consider the entire ATP cycle in Fig. 1 (in our case, for leaky vesicles with saturating ATP and the same Ca^{2+} and H^+ concentrations in and out). We then assume that three species or states, namely ATP-E, *E-P_{in}, and **E-P_{out}, are the dominant ones in our experimental conditions, and that other species listed in Fig. 1 can be neglected in this analysis. The same kind of cooperativity introduced for E in the equilibrium model will again be used for each of the three species in our condensed steady state cycle, except that here we shall deal with a two-site rather than a four-site unit and, of course, we would anticipate that the interaction parameters might be different for species mentioned above.

We designate (as indicated in Fig. 1)the three principal states in the ATPase cycle T (ATP-E), α (*E-P_{in}), and β (**E-P_{out}). Each of these has nine substates, depending on the extent of binding of Ca^{2+} and H^+. That is, E is a two-site unit: it has one ATP (catalytic) site and two domains, each of which has a site for the competitive binding of Ca^{2+} binding of Ca^{2+} and H^+. Each of the two domains (which in this model are assumed to be equivalent) can be in one of three binding states or conformations: 0 (site empty), 1 (site occupied by Ca^{2+}), or 2 (site occupied by H^+). A dimer, then, has $3 \times 3 = 9$ substates. However, because of assumed symmetry, only six substates need to be considered explicitly (i.e., substate 02 is equivalent to 20, etc.), provided appropriate factors of 2 are introduced in the rate constants to take care of this degeneracy.

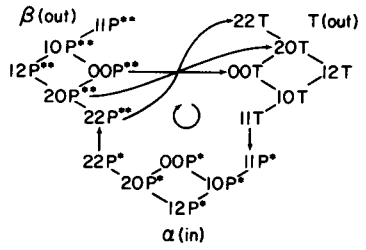

FIGURE 6 Kinetic diagram used to simulate steady state ATPase activity. States α, β, and T are also indicated in Fig. 1. See text for further details.

The kinetic diagram in Fig. 6 includes states T, α, and β, each with six substates. The two numerals in the notation of each substate indicate the binding status of the two domains. In state α, the binding sites have access to inside Ca^{2+} and H^+; in states T and β, the binding sites have access to outside Ca^{2+} and H^+. It should be pointed out that this diagram includes all possible binding relationships and orientations for the low-affinity state of the phosphoenzyme, i.e., inward oriented sites (α) interacting with Ca^{2+}, H^+, or neither, and outward oriented sites (β) interacting with Ca^{2+}, H^+, or neither. This is at variance with commonly published schemes that consider only inward orientation and interaction with Ca^{2+} (deMeis and Vianna, 1978). In our case, consideration of all species is required for the analysis below, and the probability of each species is determined by the constants chosen for the simulated reactions.

Each line in Fig. 6 represents a binding transition and its inverse. The arrows indicate transitions that we treat, for simplicity, as one-way transitions. If this model were used with native (nonleaky) vesicles where the entire system may not be far from equilibrium (nonzero Ca^{2+} and H^+ thermodynamic forces are operative, as well as the ATP force), the inverses of these one-way transitions would have to be included. In Fig. 6 as it stands, cyclic ATPase activity can occur only in the clockwise direction.

Because β and T are"out" states and α is an "in" state, it will be seen that the model in Fig. 6 exhibits tight coupling among ATP, Ca^{2+}, and H^+: in each completed cycle by one ATPase unit, one ATP molecule is hydrolyzed, two calcium ions are transported from "out" to "in" and two protons are transported from "in" to "out. " In particular, in state α, two bound protons displace two bound Ca^{2+} (the binding of Ca^{2+} is taken to be very weak in states α and β compared with state T). Similarly, in states T and β (combined), two Ca^{2+} displace two protons.

A simplification that we make below is to assume that all of the binding and release transitions within state T are relatively fast so that these substates are in internal equilibrium with each other. In effect, for computational purposes, this reduces the number of substates in Fig. 6 from 18 to 13 (T can be considered a single state provided that the equilibrium fraction of T in substate 11T is calculated). Incidentally, this simplification is in no way essential; the 18-state system is hardly more difficult to handle than the 13-state system.

In our first calculations, the only transition allowed from β to T was 00P** → 00T. However, this did not provide sufficient ATP flux at high H^+ concentrations (see the pH 6 curve in Fig. 5). Consequently, 22P** → 22T was included (with a relatively small rate constant), along with the intermediate case 20P** → 20T, for consistency.

ANALYSIS OF THE MODEL

With a complete set of rate constants for the 13-state kinetic diagram in Fig. 6, at given Ca^{2+} and H^+ concentrations, the steady state probability p_i for each of the 13 states can easily be calculated (18) by computer. Then the desired ATP flux J can be found(e.g., $J = kp_{22P*}$, where k is the rate constant for 22P* → 22P**). We turn now to the details of this procedure. The main complication is related to interactions of binding domains (i.e., cooperativity) on the rate constants. We treat this effect in the fundamental way used already in a number of other papers (19–21).

Equilibrium Binding on a Two-Site Unit

The treatment in this subsection would apply to any one of the states T, α, or β at equilibrium. It is analogous to Eqs. 1–9 of reference 3 for a four-site unit.

The grand partition function (3, 22) for a single ATPase unit is

$$\xi = x_{00} + 2K_1c_1x_{01} + 2K_2c_2x_{02} + K_1^2c_1^2x_{11} + 2K_1c_1K_2c_2x_{12} + K_2^2c_2^2x_{22}, \quad (1)$$

where $x_{ij} \equiv e^{-w_{ij}/kT}$, w_{ij} is the interaction free energy between two binding domains in states i and j (i, j =0, 1, 2), c_1 is the Ca^{2+} concentration, c_2 is the H^+ concentration, K_1 is the intrinsic binding constant for Ca^{2+} on the binding domain ("intrinsic" refers to a hypothetical isolated binding domain), and K_2 is the corresponding intrinsic binding constant for H^+. Each term in ξ represents a possible binding state of the ATPase unit and gives the relative population of that state at equilibrium. Eq. 1 can be recast in a more useful form by dividing by x_{00} and then defining (see Eqs. 7 and 8 of reference 3):

$$K_1'' \equiv K_1(x_{11}/x_{00})^{1/2}, \qquad K_2'' \equiv K_2(x_{22}/x_{00})^{1/2} \quad (2)$$

$$Y^2 \equiv (x_{01}^2/x_{11}x_{00})^{1/2}, \qquad Z^2 \equiv (x_{02}^2/x_{22}x_{00})^{1/2},$$

$$U^2 \equiv (x_{12}^2/x_{22}x_{11})^{1/2}. \quad (3)$$

This leads to

$$\xi/x_{00} = \underset{(00)}{1} + \underset{(10)}{2K_1''c_1Y^2} + \underset{(20)}{2K_2''c_2Z^2} + \underset{(11)}{K_1''^2c_1^2} + \underset{(12)}{2K_1''c_1K_2''c_2U^2} + \underset{(22)}{K_2''^2c_2^2}. \quad (4)$$

Note that there are only three effective cooperativity parameters in Eq. 4 (and that $Y^4 = y$ in reference 3, etc.).

For the physical significance of K_1'' and K_2'', see the discussion of the corresponding K_1' and K_2' in reference 3 (Eq. 9). It is easy to see, though, that K_1'' and K_2'' are the effective, operational binding constants, as follows. When $Y = Z = U = 1$, there is no cooperativity in the binding, and

$$\xi/x_{00} = (1 + K_1''c_1 + K_2''c_2)^2. \quad (5)$$

Note that $Y = Z = U = 1$ does not mean that the interaction free energies w_{ij} are zero (or that all the $x_{ij} = 1$); this would be unrealistic. Eq. 5 then gives

$$\theta = K_i''c_i/(1 + K_1''c_1 + K_2''c_2) \qquad (i = 1, 2) \quad (6)$$

for the fractional binding of ligand i. This is the well known formula for noncooperative competitive binding.

To distinguish the parameters in Eq. 4 for the three states, we use subscripts T, α, and β: K_{1T}'' K_{2T}'', Y_T, etc. There are now nine interaction parameters. Of course c_1 and c_2 are the same for the three states (because of the leaky vesicles).

The fraction of state T (assumed to be in internal equilibrium) that is in the substate 11T is, from Eq. 4,

$$f_{11T} = K_{1T}''^2 c_1^2/(1 + 2K_{1T}'' c_1 Y_T^2 + \cdots + K_{2T}''^2 c_2^2). \quad (7)$$

This relation is needed below.

Introduction of Rate Constants

The rate constants for binding and release of Ca^{2+} and H^+ in states α and β are designated α_1, α_{-1} (Ca^{2+}), α_2, α_{-2}, (H^+), β_1, β_{-1} (Ca^{2+}), β_2, β_{-2} (H^+). These are the rate constants without cooperativity or symmetry factors (see below). They are related to the binding constants already introduced by

$$\alpha_1/\alpha_{-1} = K_{1\alpha}'', \alpha_2/\alpha_{-2} = K_{2\alpha}'', \beta_1/\beta_{-1} = K_{1\beta}'', \beta_2/\beta_{-2} = K_{2\beta}''. \quad (8)$$

In our computations below, we assign values for K'', α_{-1}, α_{-2}, etc.; then the binding rate constants α_1, α_2, etc., are determined by Eq. 8.

Let us refer to the α state to introduce cooperativity and symmetry factors. In the inverse transitions 00P* ↔ 10P* (binding of Ca^{2+}), we see from Eq. 4 that the factor $2Y_\alpha^2$ has to be distributed between → and ← rate constants. The factor 2 belongs to → because there are two sites in 00P* on which to bind a Ca^{2+}. We divide the factor Y_α^2 evenly (symmetrically) between → and ← (i.e., Y_α and Y_α^{-1}, respectively). This is plausible (though arbitrary) because we consider the rate-determining feature of the binding process (for both Ca^{2+} and H^+) to be a conformational change (2, 3). (If this were simple diffusion-controlled binding, we would put 1 in → and Y_α^{-2} in ←). Thus the two first-order rate constants for the above transition pair in Fig. 6. are

$$\begin{aligned} &00P^* \rightarrow 10P^*{:}2\alpha_1 c_1 Y_\alpha \\ &00P^* \leftarrow 10P^*{:}\alpha_{-1} Y_\alpha^{-1}. \end{aligned} \quad (9)$$

As a second example, let us consider 10P* ↔ 12P* (binding of H^+) in Fig. 6. From the quotient of the 12 and 10 terms in Eq. 4,we see that there is a cooperativity factor U_α^2/Y_α^2 to be divided (evenly) between → and ← (but no symmetry factor in this case). Thus the first-order rate constants for this transition pair are

$$\begin{aligned} &10P^* \rightarrow 12P^*{:}\alpha_2 c_2 U_\alpha Y_\alpha^{-1} \\ &10P^* \leftarrow 12P^*{:}\alpha_{-2} Y_\alpha U_\alpha^{-1}. \end{aligned} \quad (10)$$

If we use the same procedure for the remaining transitions of state α in Fig. 6, we find

$$\begin{aligned} &00P^* \rightarrow 20P^*{:}2\,\alpha_2 c_2 Z_\alpha \\ &00P^* \leftarrow 20P^*{:}\alpha_{-2} Z_\alpha^{-1} \\ &20P^* \rightarrow 12P^*{:}\alpha_1 c_1 U_\alpha Z_\alpha^{-1} \\ &20P^* \leftarrow 12P^*{:}\alpha_{-1} Z_\alpha U_\alpha^{-1} \\ &20P^* \rightarrow 22P^*{:}\alpha_2 c_2 Z_\alpha^{-1} \\ &20P^* \leftarrow 22P^*{:}2\,\alpha_{-2} Z_\alpha \\ &10P^* \rightarrow 11P^*{:}\alpha_1 c_1 Y_\alpha^{-1} \\ &10P^* \leftarrow 11P^*{:}2\,\alpha_{-1} Y_\alpha. \end{aligned} \quad (11)$$

For state β, we merely replace α by β everywhere in Eqs. 9–11. Rate constants did not need to be introduced for state T because of the assumed internal equilibrium in that state.

The remaining rate constant notation used in Fig. 6 (arrows) is

$$\begin{aligned} &11T \rightarrow 11P^*{:}k_T \qquad 22P^* \rightarrow 22P^{**}{:}k \\ &00P^{**} \rightarrow 00T{:}k_{00} \qquad 20P^{**} \rightarrow 20T{:}k_{20}. \\ &22P^{**} \rightarrow 22T{:}k_{22} \end{aligned} \quad (12)$$

Because T is treated as a single equilibrium state (see above), the effective rate constant for T → 11P* is $k_T f_{11T}$ (Eq. 7). The constant k_{20} is not considered an independent parameter; we assume $k_{20} = (k_{00}k_{22})^{1/2}$, which seems plausible.

In summary, the independent parameters of the model are (not including the variable concentrations c_1 and c_2):

Binding constants	K_{1T}'', K_{2T}'', $K_{1\alpha}''$, $K_{2\alpha}''$, $K_{1\beta}''$, $K_{2\beta}''$,
Rate constants	$\alpha_{-1}, \alpha_{-2}, \beta_{-1}, \beta_{-2}, k, k_T, k_{00}, k_{22}$
Cooperativity	$Y_T, Z_T, U_T, Y_\alpha, Z_\alpha, U_\alpha, Y_\beta, Z_\beta, U_\beta$.

(13)

CALCULATIONS

There are 13 states in Fig. 6, with various possible transitions among these states. In the conventional manner (18), we can write 13 rate equations in which each dp_i/dt (i= 1, . . ., 13) is expressed as a linear combination of certain of the p_i, with rate constants as coefficients. At steady state, all of the $dp_i/dt = 0$. Thus, at steady state, we have

13 linear algebraic equations in the p_i. Actually, one of these is not independent; therefore we use 12 of these equations plus the relation $\Sigma_i p_i = 1$. This new set of 13 linear equations is then solved by computer, using matrix inversion. Then the ATP flux J (per enzyme unit comprising two calcium binding domains) can be calculated in various ways, for example, $J = kp_{22P^*}$.

Our procedure was the following: (*a*) We chose an initial plausible set of binding and rate constants (Eq. 13) based on experimental data where possible; all cooperativity parameters were set equal to unity. This was used as a reference case. A reference family of J curves, as in Fig. 5, was then computed. (*b*) All of the binding and rate constants were varied one at a time, to give new families of J curves to be compared with the reference set and with the experimental set (Fig. 5). (*c*) Using these results, we altered a number of binding and rate constants to find a much improved set of J curves (compared with Fig. 5). (*d*) We then varied the nine cooperative parameters one at a time (i.e., with values $\neq 1$) to observe their effects on the family of J curves. (*e*) On the basis of these results, we used several promising combinations of cooperativity parameters ($\neq 1$). We selected $U_T = 6.0$, $Z_\alpha = 0.1$ as the best combination tested. (*f*) The theoretical family of J curves obtained in this way was then improved by three scale changes.(*i*) K''_{1T} was altered to shift, in effect, the pCa axis so that the mid-points of the J curves (experimental and theoretical) at pH 7.2 occurred at the same pCa value. The constants $K''_{1\alpha}$ and $K''_{1\beta}$ were not changed in this process because they are so small (see below). (*ii*) K''_{2T}, $K''_{2\alpha}$, and $K''_{2\beta}$ were all multiplied by a common factor to shift the pH scale. (*iii*) All rate constants were multiplied by another common factor to alter the J scale. These scale changes are responsible for the unlikely looking set of parameters given below.

It should be clear from the above outline that we sampled, in fact, only a very small portion of the total parameter space. However, this sample was sufficient to obtain a rather good agreement with the experimental observations (Fig. 5). Further parameter sampling on the dimer model did not seem to us worthwhile in view of the fact that in our equilibrium binding work (3) a tetramer model was more satisfactory than a dimer. On the other hand, as already explained, we did not use a tetramer for our present calculations because the required order of magnitude increase in computational complexity does not seem justified at this time, in view of a number of uncertainties in the kinetic and structural details of the system, as presently understood.

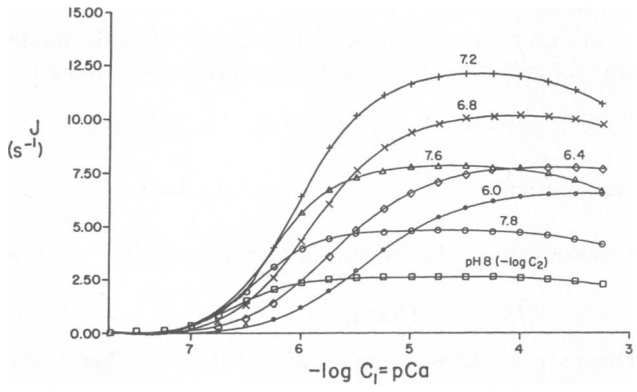

FIGURE 7 Steady state ATP flux J calculated by computer for the model in Fig. 6 and for the parameters in Eq. 14. J is plotted against pCa for several values of pH. The points connected by the lines are theoretical values derived from the simulation. These simulated curves should be compared with the experimental curves of Fig. 5.

The final parameter set used is the following:

$$\begin{aligned}
K''_{1T} &= 0.2071 \times 10^6\ M^{-1} & K''_{2\alpha} &= 90.34 \times 10^6\ M^{-1} \\
K''_{2T} &= 1.585 \times 10^6\ M^{-1} & K''_{1\beta} &= 0.15 \times 10^3\ M^{-1} \\
K''_{1\alpha} &= 0.15 \times 10^3\ M^{-1} & K''_{2\beta} &= 57.06 \times 10^6\ M^{-1} \\
\alpha_{-1} &= 163.2\ s^{-1} & k &= 261.1\ s^{-1} \\
\alpha_{-2} &= 32.63\ s^{-1} & k_T &= 978.9\ s^{-1} \\
\beta_{-1} &= 130.5\ s^{-1} & k_{00} &= 326.3\ s^{-1} \\
\beta_{-2} &= 326.3\ s^{-1} & k_{22} &= 9.463\ s^{-1} \\
U_T &= 6.0 & Z_\alpha &= 0.1. \qquad (14)
\end{aligned}$$

The other seven cooperativity parameters retain the value 1.0. The family of J curves computed from this parameter set is shown in Fig. 7. These curves should be compared with the experimental set in Fig. 5. The experimental curves are of course less complete, not reaching J_{max} at any pH. The agreement is excellent except for pH 7.8 and 8.0, where the theoretical curves rise too quickly. This discrepancy may be due at least in part to inaccurate estimates of the Ca^{2+} concentrations for the experimental curves at pH 7.8 and 8.0, since EGTA-Ca is not a satisfactory Ca^{2+} buffer at these pH levels.

Fig. 8 is for the same parameter set except that $U_T = Z_\alpha = 1$ (i.e., no cooperativity). These cooperativity parameters obviously have a large effect on the J curves. In passing from Fig. 8 to Fig. 7, $Z_\alpha = 0.1$ (positive cooperativity) is responsible for the lowering and rearrangement of the J_{max} positions, whereas $U_T = 6.0$ (negative cooperativity) spreads out the separate curves horizontally (along the pCa axis). These separate effects were deduced from the cases (not shown) $U_T = 1.0$, $Z_\alpha = 0.1$, and $U_T = 6.0$, $Z_\alpha = 1.0$.

Besides J, the computer print-out included all the p_i and f_{11T}. A study of these quantities is of course very helpful in understanding the J curves. Examples of intermediate states distributions at three different H^+ concentrations, as functions of the Ca^{2+} concentrations, are given in Table I. It is noteworthy that at low H^+ (pH 8.0) at J_{max},the only states with $p_i \geq 0.02$ are 10P* with 0.019 and 00P* with 0.911. At optimal H^+ (pH 7.2), at J_{max}, the p_i are more widely distributed. States with $p_i \geq 0.05$ are 10 P* with 0.057, 00P* with 0.287, 12P* with 0.219, 22P* with 0.046, 22P** with 0.205, and 20P** with 0.106. At high H^+ (pH 6.0), at J_{max}, states with $p_i \geq 0.02$ are 11P* with 0.020,

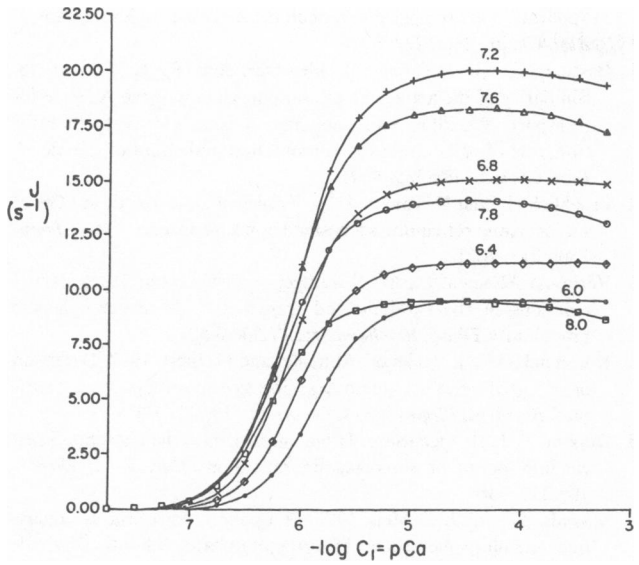

FIGURE 8 Theoretical J curves, as in Fig. 7, if all cooperativity parameters are set equal to unity.

12P* with 0.346, 22P* with 0.025, 22P** with 0.566, and 20P** with 0.020. The principal-qualitative feature in the set of experimental J curves is the increase in J_{max} from pH 8.0 to pH 7.2, followed by a decrease in J_{max} from pH 7.2 to pH 6.0. The above probabilities show that the model produces this effect in the following way. At low H^+ (pH 8.0), the α state 00P* provides a kinetic barrier to the cyclic activity both because of low H^+ and because of $Z_\alpha \leq 1$ (see the top two lines in Eq. 11). At high H^+ (pH 6.0), the β state 22P** produces a similar kinetic barrier because the rate constant k_{22} is much smaller than k_{20} (out of 20P**) and k_{00} (out of 00P**). The latter two states are not populated much because of the high H^+. At pH7.2 neither of these barriers is very effective and J_{max} is optimal.

CONCLUSIONS

In this paper we have demonstrated experimentally that the known (3) competition of H^+ and Ca^{2+} for binding to SR ATPase, is directed to specific sites whose occupancy by Ca^{2+} is an absolute requirement for enzyme activation. In fact, enzyme phosphorylation upon addition of ATP can be prevented or permitted by simply adjusting the ratio between H^+ and Ca^{2+} concentrations, so as to allow H^+ or Ca^{2+} binding to the ATPase sites (Fig. 2). This clearly explains an effect of H^+ at the beginning of the catalytic cycle, and the low ATP flux observed at high H^+ and low Ca^+ concentrations.

We have also demonstrated that at the end of the enzyme cycle, hydrolytic cleavage of the phosphoenzyme (Fig. 4) proceeds at a lower rate where the pH is low (i.e., 6.6).This explain the low ATP flux at high H^+ concentrations, even in the presence of saturating Ca^{2+} (Fig. 5).

Finally, we have demonstrated intermediate reactions related to release of Ca^{2+} from the internalized sites following enzyme phosphorylation, is inhibited when the pH is high (Fig. 3). This explains the low ATP flux at low H^+ concentration and saturating Ca^{2+} (Fig. 5).

We have then formulated a model (Fig. 6) for a reaction mechanism to explain our experimental findings. Although the model subjected to analysis is based on a reaction mechanism that is incomplete and as yet uncertain in its details, we obtained a rather satisfactory simulation of a series of experimental curves representing the complex dependence of steady state ATPase activity on Ca^{2+} and H^+ concentrations. The model includes competitive binding of Ca^{2+} and H^+ to two sites per each enzyme unit, and three main kinetic states of the reaction cycle, with 13 substates determined by occupancy of the two sites by Ca^{2+}, H^+, or neither, in each state. We were then able to demonstrate that the kinetic progression of each state is strongly influenced by the identity of the ligand (Ca^{2+} vs. H^+), with an overall pattern that is consistent with active transport of Ca^{2+} in one direction, and counterflux of H^+ in the other direction (23–26). Consistent with this mechanism, it is possible to show (Fig. 9) that addition of ATP to native SR vesicles is followed by ejection of H^+, while no H^+ ejection is noted when ATP is added to leaky vesicles (at pH 6.1, no detectable H^+ production is associated with the hydrolytic reaction). It should be pointed out that while a high Ca^{2+} gradient is formed as a consequence of active transport in native SR vesicles, the resulting "net" H^+ gradient is rather shallow, owing to the presence of effective buffers and passive fluxes through independent H^+ channels.

We also found that interaction between the two binding domains in at least two states is required to obtain satisfactory simulation of the experimental data. In the simulations presented here, this interaction is manifested by negative cooperativity in the Ca^{2+}-H^+ interactions in the T

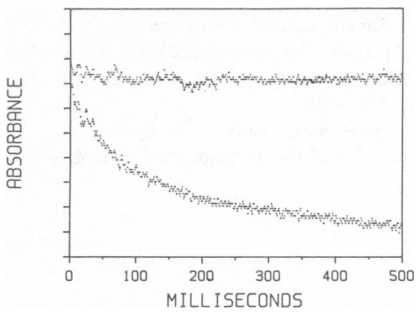

FIGURE 9 H^+ extrusion from SR vesicles following addition of ATP. The flat trace was obtained with SR vesicles rendered leaky by addition of 0.1% (vol/vol) Triton-X-100 (02 10 μM A23187). The curved trace was obtained with vesicles sustaining calcium accumulation. Medium: 80 mM KCl, 5 mM $MgCl_2$, 1.5 mM MES (pH 6.1), 40 μM chlorophenol red, 100 μM $CaCl_2$, and 1 mg of SR protein/ml. The reaction was started by the addition of 250 μM ATP in a stopped-flow apparatus, and differential absorption changes were obtained between 577 and 630 nm. This is a technically improved version of the original experiment of Chiesi and Inesi (23).

state and positive cooperativity in the presence of H^+ as the ligand in the α state (see Eq. 3).

Finally, it is noteworthy that for simplicity our model (Fig. 6) postulates that hydrolytic cleavage of the phosphoenzyme (**E-P) is inhibited by H^+ occupancy of the same sites operating the H^+ vs. Ca^{2+} exchange (Fig. 6). On the other hand, our calculations show no significant occupancy of **E-P by Ca^{2+} (Table I). Therefore, it is possible that inhibition of hydrolytic activity is related to H^+ occupancy of an independent site.

Received for publication 4 January 1983 and in final form 17 May 1983.

REFERENCES

1. deMeis, L., and A. Vianna. 1979. Energy interconversion by the Ca^{++}-dependent ATPase of the sarcoplasmic reticulum. *Annu. Rev. Biochemistry.* 48:275–292.
2. Inesi, G., M. Kurzmack, C. Coan, and D. Lewis. 1980. Cooperative calcium binding and ATPase activation in sarcoplasmic reticulum vesicles. *J. Biol. Chem.* 255:3025–3031.
3. Hill, T., and G. Inesi. 1982. Equilibrium cooperative binding of calcium and protons by sarcoplasmic reticulum ATPase. *Proc. Natl. Acad. Sci.* 79:3978–3982.
4. Eletr, S., and G. Inesi. 1972. Phospholipid orientation in sarcoplasmic reticulum membranes: spin label SR and proton NMR studies. *Biochim. Biophys. Acta.* 282:174–179.
5. Lin, T., and M. Morales. 1977. Application of a one-step procedure for measuring inorganic phosphate in the presence of proteins: the actomyosin ATPase system. *Anal. Biochem.* 77:10–17.
6. Allen, D., J. Blinks, and F. Prendergast. 1977. Aequorin luminescence: relation of light emission to calcium concentration—a calcium-independent component. *Science (Wash. D.C.).* 195:996–998.
7. Fabiato, A., and F. Fabiato. 1979. Calculator programs for computing the composition of the solutions containing multiple metals and ligands used for experiments in skinned muscle cells. *J. Physiol. (Paris).* 75:463–505.
8. Yamamoto, T., and Y. Tonomura. 1967. Reaction mechanism of the Ca^{++}-dependentATPase of sarcoplasmic reticulum from skeletal muscle. I. Kinetic studies. *J. Biochem. (Tokyo).* 62:558–575.
9. Makinose, M. 1969. The phosphorylation of the membrane protein of the sarcoplasmic vesicles during active calcium transport. *Eur. J. Biochem.* 10:74–82.
10. Degani, C., and P. Boyer. 1973. A borohydride reduction method for characterization of the acylphosphate linkage in proteins and its application to sarcoplasmic reticulum adenosine triphosphatase. *J. Biol. Chem.* 248:8222–8226.
11. Bastide, F., G. Meissner, S. Fleischer, and R. L. Post. 1973. Similarity of the active site of phosphorylation of the ATPase for transport of sodium and potassium ions in kidney to that for transport of calcium ions in sarcoplasmic reticulum of muscle. *J. Biol. Chem.* 248:8385–8391.
12. Froehlich, J., and E. Taylor. 1975. Transient state kinetic studies of sarcoplasmic reticulum adenosine triphosphatase. *J. Biol. Chem.* 250:2013–2021.
13. Verjovski-Almeida, S., M. Kurzmack, and G. Inesi. 1978. Partial reactions in the catalytic and transport cycle of sarcoplasmic reticulum ATPase. *Biochemistry.* 17:5006–5013.
14. Kurzmack, M., S. Verjovski-Almeida, and G. Inesi. 1977. Detection of an initial burst of calcium translocation in sarcoplasmic reticulum. *Biochem. Biophys. Res. Commun.* 78:772–776.
15. Dupont, Y. 1980. Occlusion of divalent cations in the phosphorylated calcium pump of sarcoplasmic reticulum. *Eur. J. Biochem.* 109:231–238.
16. Masuda, H., and L. deMeis. 1973. Phosphorylation of the sarcoplasmic reticulum membrane by orthophosphate. Inhibition by calcium ions. *Biochemistry.* 12:4581–4585.
17. McKinley, D., and G. Meissner. 1978. Evidence for a K^+, Na^+ permeable channel in sarcoplasmic-reticulum. *J. Membr. Biol.* 44:159–186.
18. Hill, T. 1977. Free Energy Transduction in Biology. Academic Press, Inc., New York.
19. Hill, T. 1977. Theoretical study of the effect of enzyme-enzyme interactions on steady-state enzymekinetics. *Proc. Natl. Acad. Sci. USA.* 74:3632–3636.
20. Hill, T. 1977. Further study of the effect of enzyme-enzyme interactions on steady-state enzyme kinetics. *Proc. Natl. Acad. Sci. USA.* 74:4111–4115.
21. Hill, T., and A. Levitzki. 1980. Subunit neighbor interactions in enzyme kinetics: half-of-the-sites reactivity in a dimer. *Proc. Natl. Acad. Sci. USA.* 77:5741–5745.
22. Hill, T. 1960. Statistical Thermodynamics. Addison-Wesley Publishing Co., Inc., Reading, MA.
23. Chiesi, M., and G. Inesi. 1980. Adenosine 5'-triphosphate dependent fluxes of manganese and hydrogen ions in sarcoplasmic reticulum vesicles. *Biochemistry.* 19:2912–2918.
24. Carvalho, A. 1972. Binding and release of cations by sarcoplasmic reticulum before and after removal of lipid. *Eur. J. Biochem.* 27:491–502.
25. Madeira, V. 1978. Proton gradient formation during transport of $Ca^{++}$by sarcoplasmic reticulum. *Arch. Biochem. Biophys.* 185:316–325.
26. Ueno, T., and T. Sekine. 1981. A role of H^+ flux in active Ca^{++} transport in sarcoplasmic reticulum vesicles. I. Effect of an artificially imposed H^+ gradient on Ca^{++} uptake. *J. Biochem. (Tokyo).* 89:1239–1246.